Deciphering the role of amine concentration on polyamide formation towards enhanced RO performance

Lu Elfa Peng,[†] Qimao Gan,[†] Zhe Yang,[†] Li Wang,[†] Peng-Fei Sun,[‡] Hao Guo,[†] Hee-Deung Park, Chuyang Y. Tang*[,†]

[†]Department of Civil Engineering, The University of Hong Kong, Pokfulam, Hong Kong SAR, China.

[‡]School of Civil, Environmental and Architectural Engineering, Korea University, Seoul, 02841, South Korea

[*]Corresponding Authors:

Chuyang Y. Tang, tangc@hku.hk, +852 28591976

21 **TABLE OF CONTENT**

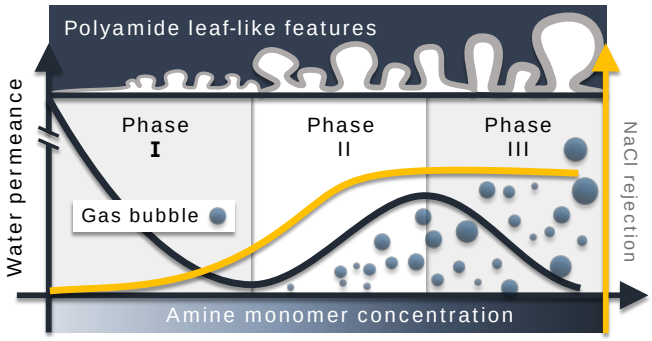

22

ABSTRACT

Polyamide surface morphology and its underneath nanosized voids have crucial influence on the separation performance of thin film composite (TFC) polyamide reverse osmosis (RO) membranes. Although there have been numerous studies reporting the impact of amine monomer concentration on polyamide formation and membrane performance, the observations and interpretations in the existing literature remain controversial. In this study, we performed interfacial polymerization (IP) of polyamide films over a wide range of *m*-phenylenediamine (MPD) concentration (0.05-8.0 w/w%). For the first time, we demonstrate that the water permeance of the resultant TFC membranes are governed by the competing effects of (1) promoted polyamide film growth for forming thicker polyamide films, and (2) improved nanofoaming effect that results in more extensive nanovoids at higher MPD concentrations. To dissect these competing mechanisms, we further adopted a free-interface IP strategy to suppress the nanofoaming effect. The corresponding polyamide nanofilms had negligible nanovoids and monotonously increased film thickness, leading to decreased water permeance at high MPD concentrations. In contrast, the conventional TFC membranes exhibited optimal water permeance at the intermediate MPD concentration of 2.0 w/w%, which results from the tradeoff between improved nanovoid formation (which promotes higher permeance) and increased film growth (which limits permeance). On the other hand, the better film growth at greater MPD concentration was generally beneficial for achieving better membrane rejection. The current study unveils the fundamental chemistry-morphology-performance relationship of TFC polyamide membranes and provides important implications on their synthesis and environmental applications.

Keywords: Reverse osmosis membrane; polyamide film; interfacial polymerization; amine concentration; nanofoaming theory.

INTRODUCTION

To address global water shortage and pollution issues, reverse osmosis (RO) technology has been playing a crucial role in desalination and water reuse.[1-3] Modern RO membranes adopt a thin film composite (TFC) structure with a polyamide functional film on top of a porous substrate. To prepare an RO membrane, typically an amine monomer (e.g., *m*-phenylenediamine (MPD)) water solution is first applied to impregnate the porous substrate, followed by adding a trimesoyl chloride (TMC) organic solution (e.g., in hexane). The interfacial polymerization (IP) of these two monomers forms a polyamide thin film on the substrate. This polyamide film commonly presents "ridge-and-valley" roughness features[4-6] containing numerous nano-sized voids of a few nanometers to several hundred nanometers.[7-16] These nanovoids are well correlated with the separation performance of RO membranes.[9-12, 17, 18]

To tailor these features towards better membrane performance, amine monomer concentration has been commonly investigated as a fundamental and crucial parameter in literature.[19-25] Some studies reported that increasing amine concentration can lead to monotonously decreased water permeance of polyamide membranes (under a fixed TMC concentration),[5, 20, 22, 26, 27] whereas, an opposite trend of increased permeance was also reported.[28] Interestingly, some researchers observed that water permeance first climbs up and then declines as amine concentration increases.[23-25, 29, 30] However, despite these well-documented experimental observations, the governing mechanism(s) remain poorly understood.

Recently, Tang and coworkers[31-36] proposed a nanofoaming theory to explain the

formation of nanovoids within the polyamide layer, which may provide a novel angle to decipher the role of amine concentration. According to this theory, the heat and H^+ generated in the IP reaction (Figure 1A) promote nanobubble formation via (1) interfacial degassing from the aqueous phase[31, 33] ($HCO_3^- + H^+ \xrightarrow{\Delta} CO_2\uparrow + H_2O$)[34] and (2) interfacial vaporization of volatile organic solvents,[36] both enhancing the formation of nanovoids. Furthermore, Song et al.[32] reported that the formation of these nanovoids is largely dependent on the confinement effect by the substrate. For IP reactions without a substrate, the bubbles can escape from the "free interface", resulting in a smooth polyamide morphology with few nanovoids.[32, 35, 37] Recently, Grzebyk et al.[38] fabricated additional polyamide layer atop existing TFC polyamide membranes by supplying MPD through the existing polyamide film. In this case, the existing polyamide film acted as a substrate with a strong confinement effect, atop which the subsequently formed additional polyamide layer exhibited more prominent nanovoids. The nanofoaming theory prompts us to re-examine the role of amine concentration on nanovoid formation which not only tailors the polyamide morphology but also regulates its separation performance.

Herein, we decipher the fundamental role of amine concentration on polyamide membrane formation over a wide range of MPD concentration (0.05-8.0 w/w%). To dissect the critical importance of interfacial degassing/vaporization during the IP reaction, we adopt a free interface IP strategy to suppress nanovoid formation.[32, 35-37] By contrasting polyamide films formed at a free interface with those prepared on a conventional substrate, we demonstrate for the first time that increasing MPD concentration promotes the competition between improved nanofoaming and enhanced polyamide film growth. These competing mechanisms regulate the separation

performance of the resultant membranes (Figure 1B), which has major implications to their environmental applications. Our study unveils the fundamental chemistry-morphology-performance relationship of TFC polyamide RO membranes and provides important guides on membrane design and synthesis.

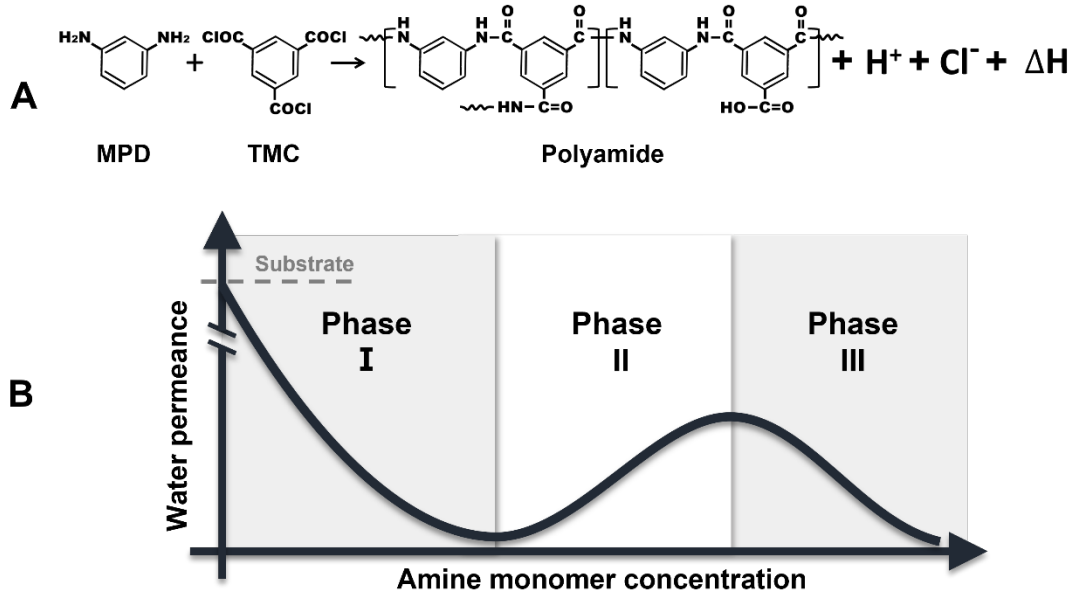

Figure 1. (A) IP reaction between MPD and TMC generates acid and heat as byproducts. (B) The effect of amine monomer concentration on the water permeance of TFC membranes.

METHODOLOGY

Chemicals and materials. MPD (99%), TMC (98%) and *n*-hexane (HPLC grade, ≥95%) were purchased from Sigma-Aldrich and used to prepare polyamide thin films. Commercial polysulfone (PSf) ultrafiltration membranes (MWCO 67 kDa, Vontron Technology) were used as substrates to prepare TFC membranes. Glycerol (Dieckmann) was used for membrane sample treatment. Sodium chloride (NaCl, Dieckmann), boric acid ($B(OH)_3$, Dieckmann) and arsenic(III) oxide (As_2O_3, ≥99.0%, Sigma-Aldrich) were used for membrane performance tests. All aqueous solutions were prepared using Milli-Q water (Elix Essential).

Freestanding polyamide film synthesis. To suppress the formation of nanovoids, we prepared polyamide thin films at a free interface. Briefly, an MPD water solution (0.05, 0.2, 0.5, 1.0, 2.0, or 8.0 w/w%) and a 0.1 w/w% TMC/hexane solution were applied to react for 1 min at the aqueous/hexane interface without the use of a substrate following the method reported by Song et al. [32, 35-37] The unreacted MPD water solution was then removed and the formed polyamide film was loaded onto a PSf substrate via vacuum suction. The resulted membrane was rinsed by hexane to remove the excess TMC solution. This series of membranes were denoted as PAfi-MPD concentration, e.g., PAfi-0.05 for the one prepared using 0.05 w/w% MPD/water solution.

TFC polyamide membrane synthesis. Conventional TFC membranes were prepared by performing IP between a series of MPD/water solution (in concentrations of 0.05, 0.2, 0.5, 1.0, 2.0, and 8.0 w/w% that matched those used for the free-standing polyamide films) and 0.1 w/w% TMC/hexane solution on a PSf substrate. Additional MPD concentrations of 4.0, 6.0, and 10.0 w/w% were also included to confirm the trend of

membrane water permeance. In brief, a substrate was first impregnated by an MPD solution for 2 min before removing the excess solution by a rubber roller. A TMC solution was then applied on to the MPD-impregnated substrate for 1 min to form the polyamide thin film. The resulted polyamide membrane was then rinsed by hexane and was placed in a 50 °C water bath for 10 min for further polymerization. The synthesized TFC membranes were named as TFC-MPD concentration, e.g., TFC-0.05 for the one prepared using 0.05 w/w% MPD/water solution.

Membrane characterization. Field-emission scanning electron microscopy (FE-SEM, S-4800, Hitachi) operated at an accelerating voltage of 5.0 kV was applied to characterize membrane surface morphology. Samples were dried and sputter coated with a thin layer of gold before the SEM characterization. Transmission electron microscopy (TEM, CM100, Philips) operated at an accelerating voltage of 100 kV was used to resolve the membrane cross-sectional structure. Samples were soaked in 10 v/v% glycerol/water for 1 h and dried[32] before the TEM characterization. Atomic force microscopy (AFM, MFP-3D, Asylum Research) with a scanning area of 10 × 10 μm^2 was employed to measure membranes surface roughness. X-ray photoelectron spectroscopy (XPS, ULVAC-PHI X-tool) with a spectra range of 0–1400 eV was applied to analyze the elemental composition of membranes surface. The obtained atomic percent of O and N were used to calculate the ratio of oxygen to nitrogen (O/N). A ζ potential analyzer (EKA, SurPASS 3, Anton Paar) was used to measure the surface charge of polyamide films in a 1.0 mM potassium chloride background solution with a pH range of 3.0−10.0. A contact angle meter (Attension Theta Lite, Bolin Scientific) and an attenuated total reflectance Fourier transform infrared spectroscopy (ATR-FTIR, Nicolet iS5, Thermo Fisher Scientific) were applied for measuring surface

hydrophilicity and functional groups of polyamide films, respectively.

Membrane separation performance evaluation. A laboratory-scale cross-flow RO filtration system (as detailed in our previous work[34]) was used to measure water flux and solutes rejection (2000 ppm NaCl, 5 ppm boron, or 1 ppm As(III), separately) of the membranes at room temperature (~25 °C). The pH values of feed solutions were ~pH6.2 for pure water, boron solution, and As(III) solution, and ~pH6.5 for NaCl solution. A membrane cell with effective filtration area of 12.0 cm^2 was used, and the membrane coupon was pre-compacted at 17.0 bar with a cross-flow velocity of 22.4 cm/s for 2 h. Water flux and salt rejection were then tested at 15.5 bar. The water flux (J_v) and permeability (A) are calculated by:

$$J_v = \frac{\Delta m}{\Delta t \times a \times \rho} \quad (1)$$

$$A = \frac{J_v}{\Delta P - \Delta \pi} \quad (2)$$

where Δm is the mass of permeate over a time interval (Δt), a is the effective membrane area, ρ is water density, ΔP is the transmembrane pressure, and $\Delta \pi$ is the transmembrane osmotic pressure. The rejection (R) and permeability (B) of solutes were obtained from:

$$R = \frac{C_f - C_p}{C_f} \times 100\% \quad (3)$$

$$B = (\frac{1}{R} - 1) \times J_v \quad (4)$$

where C_f and C_p are solute concentrations in the feed and the permeate respectively. NaCl concentrations were determined based on conductivity measurements (Ultrameter II, Myron L). The trace contaminants (boron and As(III)) concentrations were determined by inductively coupled plasma spectrometry (ICP-MS, Agilent 7900).

RESULTS AND DISCUSSION

Microscopy on polyamide morphology of PAfi and TFC membranes

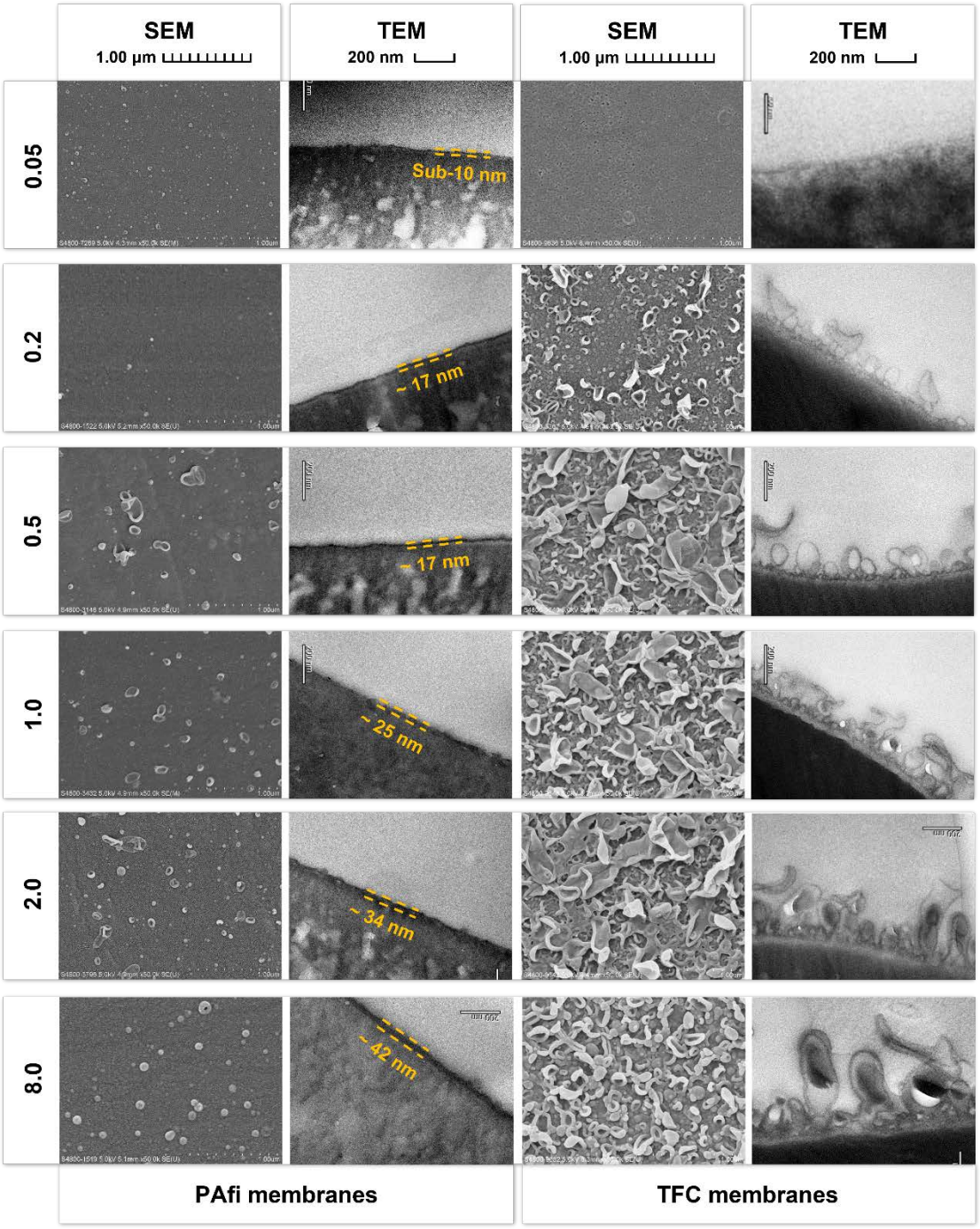

Figure 2. SEM (top views) and TEM (cross-sections) of the PAfi and TFC membranes. The numbers on the left side (0.05-8.0) represent the MPD concentrations (w/w%). The polyamide film thickness of PAfi membranes was measured using the software of *ImageJ*.

In order to resolve the mechanisms governing the role of MPD, we prepared polyamide thin films at a free interface for a series of MPD concentrations (PAfi-0.05 ~ PAfi-8.0). According to prior studies, the lack of confinement effect at the free interface would allow gas bubbles resulting from interfacial degassing/vaporization to freely escape,[32, 35, 36] which suppresses the formation of nanovoids within polyamide layers. Consequently, the PAfi membranes can serve as an ideal control series that is not affected by the nanofoaming mechanism. As expected, these PAfi membranes generally show relatively smooth surfaces (SEM images, the 1st column of Figure 2) with negligible presence of nanovoids (TEM images, the 2nd column of Figure 2). In addition, the TEM micrographs further reveal monotonously increased polyamide film thickness from sub-10 nm of PAfi-0.05 to approximately 42 nm of PAfi-8.0. This observation confirms the importance of MPD concentration on the growth of polyamide film.[19, 25, 39-41]

In contrast to the relatively flat surfaces of the PAfi series, the TFC membranes prepared on a conventional substrate generally show rough membrane surfaces with the exception for TFC-0.05 (SEM micrographs, the 3rd column of Figure 2). These rough surfaces are due to the nanovoids within the polyamide films (TEM micrographs, the 4th column of Figure 2), whose formation can be possibly attributed to the interfacial degassing/vaporization of nanosized gas bubbles.[31, 33, 34, 36] According to the works from Ma et al. and Peng et al., pre-degassing of the aqueous MPD solution[31] or decreasing of aqueous solution pH,[34] which minimizes the amount of dissolved CO_2 in the MPD solution and thus suppresses its degassing during the IP reaction, can reduce the formation of nanovoids. On the other hand, applying $NaHCO_3$ as a CO_2 precursor[33] or

using more volatile solvents as the organic phase[36] can contribute to more extensive nanovoids within the polyamide layer. Accordingly, in the current study, the smooth surface of TFC-0.05 can be attributed to the reduced interfacial heating and thus less gas/vapor production at this low monomer concentration.[31] Indeed, the MPD concentration of 0.05 w/w% may not even be sufficient to form an intact polyamide film, with some regions in the SEM image of TFC-0.05 clearly showing pores of the substrate. By increasing MPD concentration from 0.05 to 2 w/w%, the TFC membrane surfaces became increasingly rough (Figure 2 and Figure 3), along with more extensive nodules and leaf-like structures that are closely associated with nanovoids[7, 9, 11, 12] (see TEM of TFC membranes, Figure 2). TFC-0.05 had no clearly visible nanovoids. Meanwhile, the average diameter of nanovoid increased from ~51 nm for TFC-0.2 to ~100 nm for TFC-2.0 (Figure S2 in Supporting Information S2), which is accompanied with greater apparent polyamide layer thickness. Accordingly, the volume fraction of nanovoids over their total polyamide volume increased from ~26% for TFC-0.2 to 45% for TFC-2.0. The greater presence of nanovoids can be attributed to greater availability of MPD monomers for the IP reaction, leading to more reaction byproducts (i.e., heat and H^+) that favor more extensive nanofoaming by interfacial degassing[31, 34] and interfacial vaporization.[36] This trend is consistent with the work by Grzebyk et al.[38] who reported that increased concentration or continuous replenishment of MPD supply led to more prominent nanovoids within the polyamide layer.

Interestingly, TEM cross-sectional micrograph of TFC-8.0 shows more extensive and elongated roughness leaves enclosing larger nanovoids, even though its SEM surface micrograph appears to present small lateral dimensions for roughness features (Figure 2). This apparent mismatch can be explained by the greater aspect ratio of the roughness

leaves of TFC-8.0, with the nanovoids preferentially growing in vertical direction with a narrower horizontal base. In addition, low-magnification SEM image also shows the sporadic presence of larger leaves for TFC-8.0 (Supporting Information S1), which is in good agreement with its AFM micrograph (Figure 3).

The TEM cross-sectional micrographs of TFC membranes further reveal a general trend of increased intrinsic thickness of polyamide films at higher MPD concentrations, even though it was difficult to determine their exact values. This trend is consistent with the increased film thickness observed for the PAfi series, once again highlighting the promoted polyamide film growth with increased MPD supply. A previous experimental study reported that a higher MPD concentration not only can result in an initially thicker polyamide film but also may accelerate the formation of an intact polyamide film.[40] Nevertheless, in contrast to the simple monotonic growth of polyamide films for PAfi membranes, the film growth of TFC membranes involves both enhanced thickness and promoted nanofoaming, which may result in competing effects on the water permeance (see the section on separation performance of PAfi and TFC membranes).

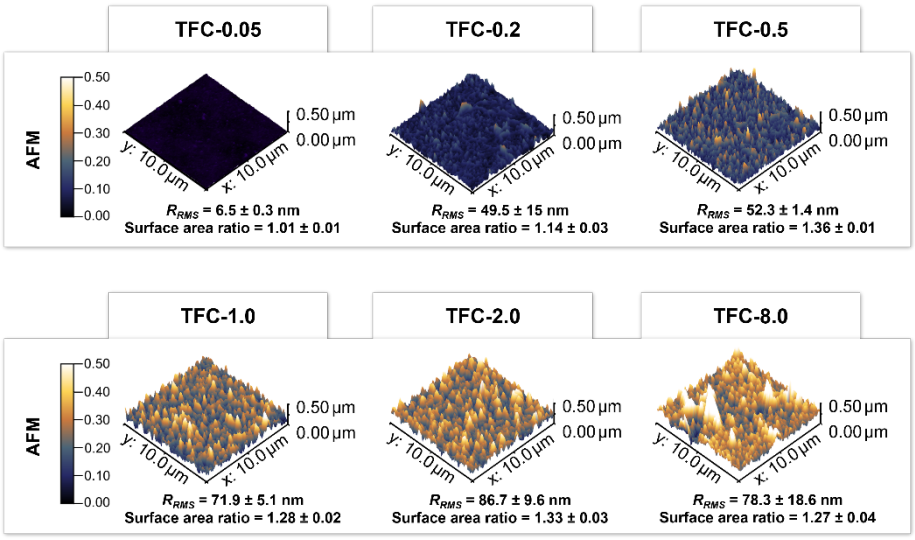

Figure 3. AFM 3D graphs of TFC membranes.

Surface chemical properties of TFC membranes

The ratio of oxygen to nitrogen (i.e., O/N ratio calculated from XPS results) on TFC membrane surfaces decreased from 3.2 ± 0.8 of TFC-0.05 to 1.5 ± 0.1 of TFC-2.0 (Figure 4A). This can be attributed to higher availability of MPD monomers in the IP reaction, which could introduce more nitrogen into the polyamide film. According to the literature,[6, 18, 42] the O/N ratio is normally in a range of 1-2, with a lower value indicating a more crosslinked rejection layer (Figure S5). However, TFC-0.05 gave an abnormally high O/N ratio of 3.2 ± 0.8. This peculiar result can partially be explained by the incomplete polyamide coverage of substrate since sulfur signal from the polysulfone substrate was detected on TFC-0.05. The polysulfone can contribute oxygen atoms to the high O/N ratio of TFC-0.05. In addition, after subtracting the number of oxygen atoms from the polysulfone substrate, the calibrated O/N ratio of TFC-0.05 was still larger than 2 (see Supporting Information S4). This high O/N ratio can be partially attributed to the extremely low availability of MPD monomers, leading to large numbers of oligo-amide (or short-chain polyamide) with many terminal carboxyl groups from TMC monomers. Increased MPD concentration up to 2.0 w/w% significantly reduced the O/N ratio, implying a more crosslinked polyamide film.

Interestingly, the TFC-8.0 prepared with abundant MPD supply also gave a high O/N ratio of 1.9 ± 0.6 with a large variation. This is possibly due to the non-uniformity of polyamide formation.[40, 41, 43] Matthews et al.[40] analyzed the density distribution of polyamide layer by Rutherford backscattering spectrometry (RBS) and found non-uniform areal layer density. Similar heterogeneous distribution of O/N ratios and carboxylates within the polyamide layer has been widely observed on some commercial

polyamide membranes.[18, 44, 45] Given the limited penetration depth of XPS characterization (< 10 nm) and the relatively thick polyamide layer of TFC-8.0, the O/N ratio for this membrane only reflects its top surface but not the entire polyamide film. Presumably, the extremely high MPD concentration can potentially promote a nearly instant formation of an intact polyamide film[46] in some locations, which can slow down the subsequent diffusion of MPD molecules through the film, creating an MPD-lean/TMC-rich environment for the IP reaction front (i.e., over the TMC-dissolved organic phase) and promoting more surface carboxyl groups to result in higher O/N ratio. In addition, the structure of polyamide layer prepared using a high MPD concentration can be more complicated than using a normal concentration. For example, Jian et al.[25] observed multiple films of the polyamide layer prepared by using high MPD concentrations. The extremely rapid formation of polyamide at very high MPD concentration could likely result in some localized defects,[32] and the subsequent diffusion of high-concentration MPD through the defects can induce the formation of additional polyamide layer. This explanation is supported by the recent experimental observation of the growth of additional (new) roughness features on an existing polyamide membrane by supplying sufficient MPD on its support side and TMC on the other side.[38]

In respect to surface charge and hydrophilicity, the TFC membranes prepared by increased MPD concentration from 0.05 to 2.0 w/w% generally present less negative charged (Figure 4B) and more hydrophobic membrane surfaces (Figure 4C). These trends are consistent with the decreased O/N ratios and can be readily explained by the less carboxyl terminal groups on the resultant polyamide layers. On the other side, TFC-8.0 gave a relatively more negatively charged and more hydrophilic membrane surface

compared to TFC-2.0, which is consistent with its high O/N ratio (indicating more carboxyl groups on the surface of TFC-8.0).

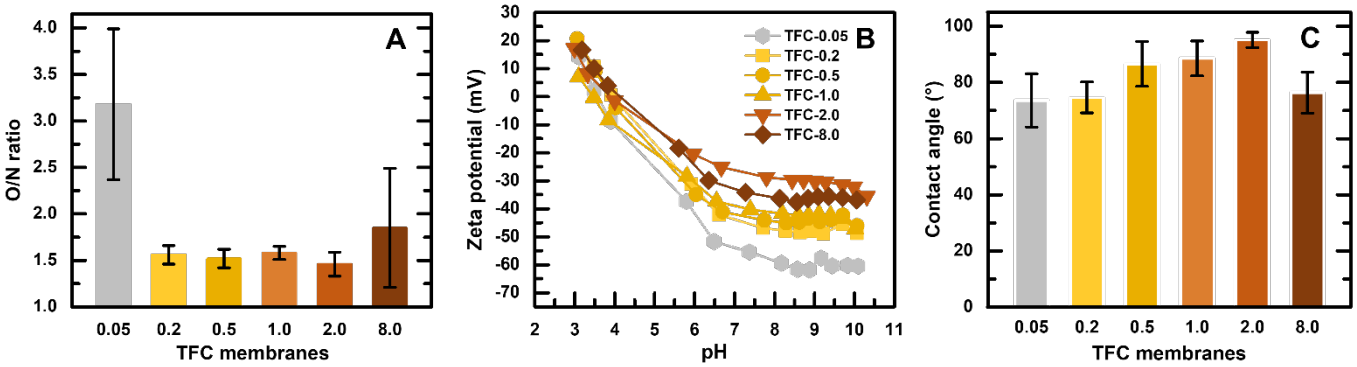

Figure 4. Surface properties of TFC membranes including (A) the ratio of oxygen to nitrogen (i.e., the O/N ratio), (B) surface charge, and (C) surface hydrophilicity.

Separation performance of PAfi and TFC membranes

PAfi membranes generally present a nearly monotonously decreased water permeance (Figure 5A), which can be attributed to their thicker polyamide films (the 2nd column in Figure 2) resulted from the promoted polyamide film growth by increasing MPD concentration. Presumably, one would have expected a similar trend for the TFC membranes. Nevertheless, the experimental results show an increase in water permeance over the MPD concentration range of 0.2-2.0 w/w%, even though the value decreased again over the MPD concentration range of 2.0-10.0 w/w% (Figure 5B). It is important to note that the formation of the TFC series is governed by both the nano-foaming mechanism and the promoted polyamide growth, yet nano-foaming is suppressed for the control PAfi series. Therefore, while the overall decreasing trend of the water permeance is well explained by the formation of thicker and more intact polyamide films, the rebound in permeance of TFC membranes over the intermediate MPD concentrations can be attributed to the more extensive nanovoids in their polyamide layers (the 4th column in Figure 2). These nanovoids along with greater layer

roughness can provide more effective surface area of polyamide films for water permeation[18] (Figure 3) and potential gutter effect for directing the water transport pathways,[37, 47] both of which favor more effective water transport towards higher water permeance. In the current study, TFC-2.0 exhibited the greatest water permeance, and this membrane also had the largest average size as well as the greatest volume fraction of nanovoids (Figure S2 in Supporting Information S2). Further analysis shows a good correlation (1) between water permeance and average diameter of nanovoids with R^2 = 0.78 and (2) between water permeance and volume fraction of nanovoids (Figure 6). The positive effect of nanovoids can be partially explained by the gutter effect that shortens the effective transport pathways of water through the polyamide film (Supporting Information S3).[37, 48, 49] Nevertheless, despite the extensive nanovoids in the polyamide layer of TFC-8.0, its increased polyamide film thickness may offset the benefit from the nanovoids, leading to declined water permeance.

For membrane rejection, both PAfi membranes and TFC membranes generally had higher NaCl rejection with increasing MPD concentration (Figure 5A, B), consistent with the improved growth of polyamide films at higher MPD concentrations. However, TFC membranes formed with low MPD concentrations (0.05, 0.2, and 0.5 w/w%) appeared to have significantly lower NaCl rejections compared to their PAfi counterparts, which might be explained by the limited MPD storage in their substrate pores[34] (compared to virtually unlimited MPD supply for the case of free interface IP). The difference in rejection values between the TFC and PAfi counterparts became negligible when the MPD concentration was ≥ 1.0 w/w%. It is worthwhile to note that some prior studies[32, 50] have reported poorer rejections for polyamide formed at free interfaces, citing the greater tendency of defect formation as the key reason.

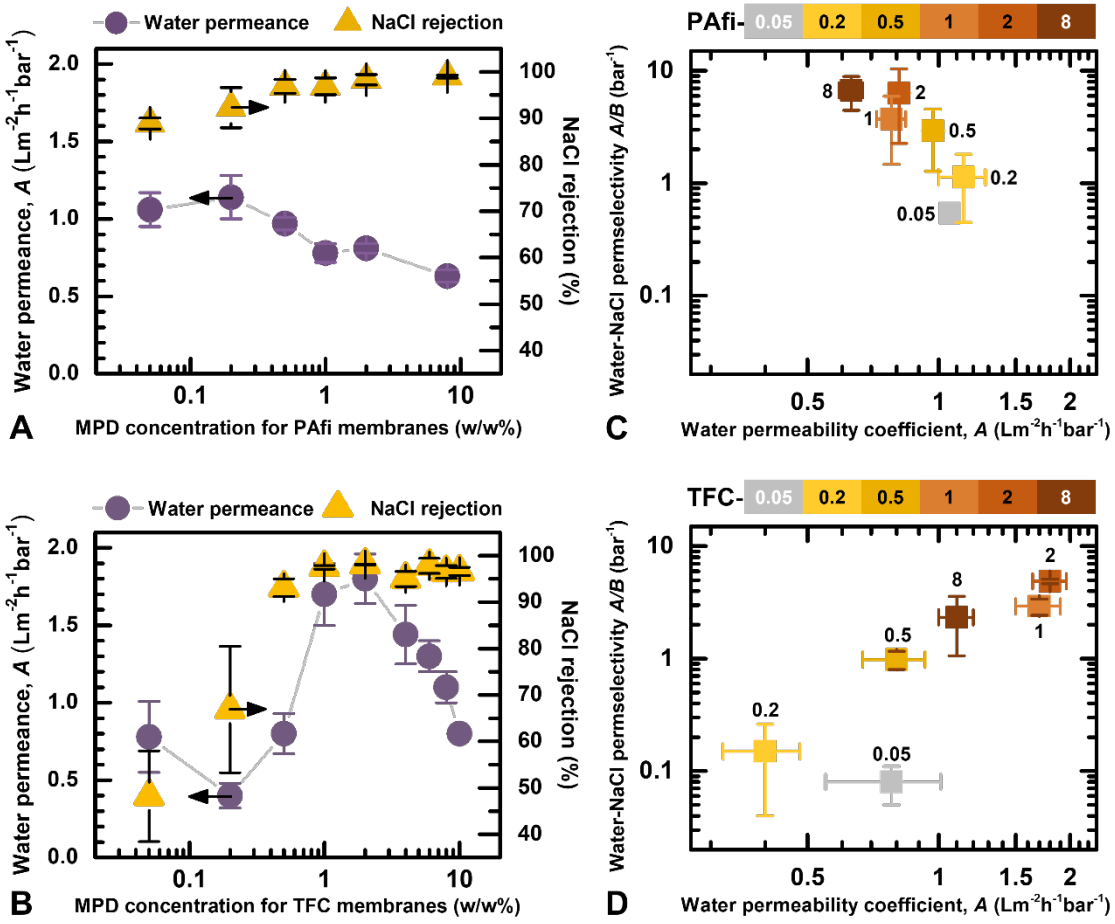

Figure 5. Water permeance and NaCl rejection of (A) PAfi membranes and (B) TFC membranes. Water/NaCl permselectivity versus water permeability for (C) PAfi membranes and (D) TFC membranes. The permselectivity *A/B* of RO membranes is given by the ratio of water permeability coefficient *A* and solute (NaCl) permeability coefficient *B*.[51, 52] Water permeance values were obtained based on the filtration tests of pure water (~pH 6.2), and NaCl rejection was obtained based on the filtration of 2000 ppm NaCl solution (~ pH6.5).

Figure 5C and Figure 5D present the water/NaCl permselectivity (*A*/*B*) versus water permeability (*A*) for PAfi and TFC membranes, respectively. The PAfi membranes generally show a strong tradeoff between their water permeance and water/NaCl permselectivity, such that increasing salt rejection was at the expense of sacrificing permeance.[51-54] More MPD monomers can contribute to increased film quality (less defects and better crosslinking) with higher NaCl rejection but meanwhile a thicker film

with lower water permeance. In contrast, increasing MPD concentration in the case TFC membranes offers the opportunity for improved water permeability in addition to better water/NaCl permselectivity (Figure 5D), thanks to the more extensive nanovoids in their polyamide layers.

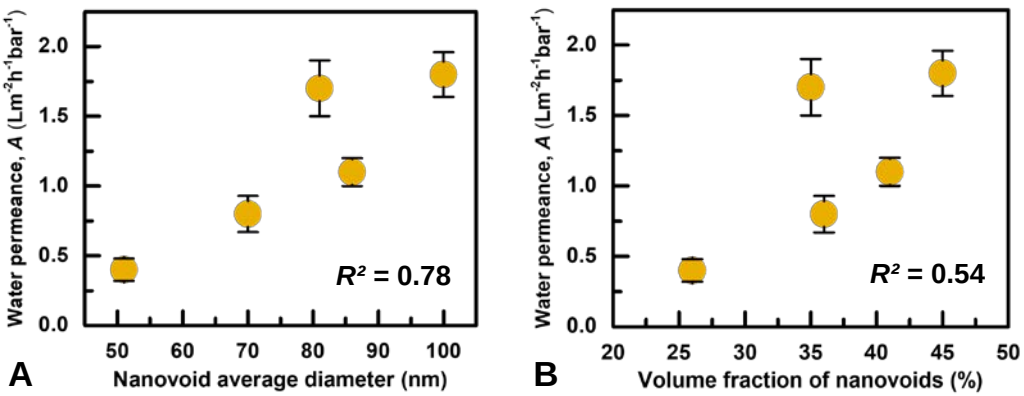

Figure 6. Correlation between water permeance and nanovoid properties: (A) nanovoid diameter; (B) volume fraction of nanovoids. The nanovoid properties are presented in Supporting Information S2.

IMPLICATIONS

The current study deciphers the fundamental role of MPD concentration on the formation of TFC polyamide RO membranes. We highlight the two fundamental mechanisms (improved polyamide film growth and nanofoaming) in regulating the membrane separation performance. Generally, increasing MPD concentration can lead to enhanced integrity of polyamide films and thus promoted NaCl rejection, thanks to the improved polyamide film growth. At the same time, the water permeance of a TFC membrane is governed by the competing effects of improved nanovoid formation (which promotes higher permeance) and increased film growth (which limits permeance). This tradeoff resulted in an optimized water permeance at 2.0 w/w% MPD concentration. The comparison between the TFC membranes and their PAfi counterparts confirms the important contribution of nanovoids toward better water permeance.

It should be noted that the optimal MPD concentration to achieve maximized water permeance could be potentially dependent on the substrate properties, particularly the ability for retaining nanobubbles generated by interfacial degassing/vaporization.[31, 34, 36] Indeed, the free interface can be idealized as a substrate with infinitely large pores with very weak confinement effect, resulting in negligible benefit of nanofoaming. On the other hand, the beneficial effect of nanofoaming could be potentially further enhanced by adopting substrates with greater confinement effect.[35] In addition, the choice of substrate would affect the MPD storage,[35] thereby regulating the intensity of nanofoaming and quality of polyamide film growth. For example, applying a substrate with smaller pores and higher pore number density can comprise stronger confinement effect and higher MPD storage to form more prominent nanovoids.[35] Recently, Grzebyk

et al.[38] performed an IP reaction on commercial TFC membranes by continuously supplying MPD to grow additional polyamide atop the existing polyamide layer of these membranes. In this case, this existing polyamide layer can be regarded as a substrate with strong confinement effect, while the continuous MPD supply can be regarded as an ideal reservoir for MPD storage. The additional polyamide layer had more prominent nanovoids compared to the existing (underneath) layer. Nevertheless, the growth of additional polyamide layer in Grzebyk et al.'s study may not improve the water permeance despite their greater nanovoids, since the new layer would introduce additional hydraulic resistance. Therefore, the role of substrate in controlling these competing mechanisms needs to be further investigated for future membrane optimization works.

In the RO literature, it is commonly known that membrane separation performance is constrained by a water permeance-permselectivity tradeoff.[51-53, 55] Here, we demonstrate the potential of tailoring nanofoaming for simultaneously enhanced water permeance and salt rejection (Figure 5D, also see ref.[33]). To be noticed, the ideal membrane properties often depend on the specific applications. For example, seawater desalination places greater emphasis on high NaCl rejection than high water permeance,[1] while water reuse calls for high water permeance in addition to salt rejection.[56] In addition, many environmental applications could be limited by inadequate rejection of harmful trace contaminants (e.g., boron in seawater desalination,[57] arsenic in groundwater treatment,[58, 59] and organic micropollutants[60, 61]). Although the current study focuses primarily on water permeance and NaCl rejection, the MPD concentration can also have even greater impacts on the rejection of some small neutral compounds such as boron and As(III) that are of great practical

importance (Figure 7). This observation reveals the greatly improved size exclusion effect resulting from the enhanced film growth at higher MPD concentration. Therefore, the choice of optimal membrane is greatly affected by the type of practical applications. For example, even though TFC-8.0 gave lower water permeance than TFC-2.0 (Figure 5B), it could potentially be a better candidate for boron removal in seawater desalination and arsenic removal from groundwater. Our study provides an important basis for tailoring application-targeted design of TFC RO membranes based on the fundamental chemistry-morphology-performance relationship.

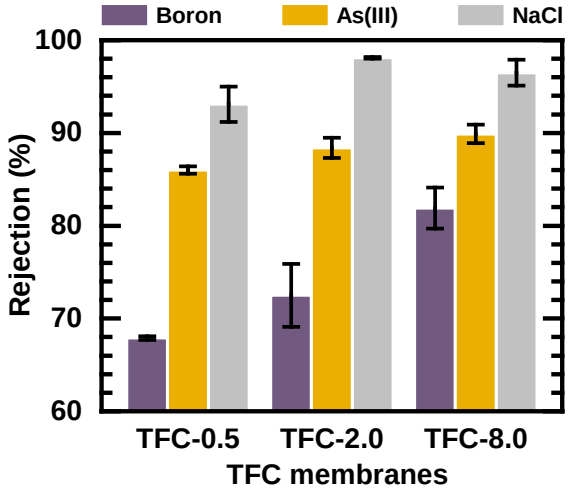

Figure 7. TFC membrane rejections to boron, As(III), and NaCl. The pH values of feed solutions were ~pH6.2 for boron and As(III), and ~pH6.5 for NaCl.

SUPPORTING INFORMATION

S1. Low-magnification SEM graphs of TFC membranes; S2. Properties of nanovoids within polyamide layers of TFC membranes; S3. Gutter effect of nanovoid; S4. Calculation of O/N ratio based on polyamide molecular structures; S5. ATR-FTIR spectra results of TFC membranes. This material is available free of charge via the Internet at http://pubs.acs.org.ssss

ACKNOWLEDGMENTS

The work is fully supported by a grant from the Research Grants Council of the Hong Kong Special Administration Region, China (SRFS2021-7S04).

REFERENCES

1. Elimelech, M.; Phillip, W. A., The future of seawater desalination: energy, technology, and the environment. *Science* **2011,** *333*, (6043), 712-7.
2. Tang, C. Y.; Yang, Z.; Guo, H.; Wen, J. J.; Nghiem, L. D.; Cornelissen, E., Potable Water Reuse through Advanced Membrane Technology. *Environ. Sci. Technol.* **2018,** *52*, (18), 10215-10223.
3. Qasim, M.; Badrelzaman, M.; Darwish, N. N.; Darwish, N. A.; Hilal, N., Reverse osmosis desalination: A state-of-the-art review. *Desalination* **2019,** *459*, 59-104.
4. Elimelech, M.; Zhu, X. H.; Childress, A. E.; Hong, S. K., Role of membrane surface morphology in colloidal fouling of cellulose acetate and composite aromatic polyamide reverse osmosis membranes. *J. Membr. Sci.* **1997,** *127*, (1), 101-109.
5. Roh, I. J.; Greenberg, A. R.; Khare, V. P., Synthesis and characterization of interfacially polymerized polyamide thin films. *Desalination* **2006,** *191*, (1-3), 279-290.
6. Tang, C. Y. Y.; Kwon, Y. N.; Leckie, J. O., Probing the nano- and micro-scales of reverse osmosis membranes - A comprehensive characterization of physiochemical properties of uncoated and coated membranes by XPS, TEM, ATR-FTIR, and streaming potential measurements. *J. Membr. Sci.* **2007,** *287*, (1), 146-156.
7. Pacheco, F. A.; Pinnau, I.; Reinhard, M.; Leckie, J. O., Characterization of isolated polyamide thin films of RO and NF membranes using novel TEM techniques. *J. Membr. Sci.* **2010,** *358*, (1-2), 51-59.
8. Yan, H.; Miao, X.; Xu, J.; Pan, G.; Zhang, Y.; Shi, Y.; Guo, M.; Liu, Y., The porous structure of the fully-aromatic polyamide film in reverse osmosis membranes. *J. Membr. Sci.* **2015,** *475*, 504-510.
9. Lin, L.; Lopez, R.; Ramon, G. Z.; Coronell, O., Investigating the void structure of the polyamide active layers of thin-film composite membranes. *J. Membr. Sci.* **2016,** *497*, 365-376.
10. Kłosowski, M. M.; McGilvery, C. M.; Li, Y.; Abellan, P.; Ramasse, Q.; Cabral, J. T.; Livingston, A. G.; Porter, A. E., Micro-to nano-scale characterisation of polyamide structures of the SW30HR RO membrane using advanced electron microscopy and stain tracers. *J. Membr. Sci.* **2016,** *520*, 465-476.
11. Wong, M. C. Y.; Lin, L.; Coronell, O.; Hoek, E. M. V.; Ramon, G. Z., Impact of liquid-filled voids within the active layer on transport through thin-film composite membranes. *J. Membr. Sci.* **2016,** *500*, 124-135.
12. Pacheco, F.; Sougrat, R.; Reinhard, M.; Leckie, J. O.; Pinnau, I., 3D visualization of the internal nanostructure of polyamide thin films in RO membranes. *J. Membr. Sci.* **2016,** *501*, 33-44.
13. Shen, L.; Hung, W.-s.; Zuo, J.; Zhang, X.; Lai, J.-Y.; Wang, Y., High-performance thin-film composite polyamide membranes developed with green ultrasound-assisted interfacial polymerization. *J. Membr. Sci.* **2019,** *570-571*, 112-119.
14. Yuan, B.; Zhao, S.; Hu, P.; Cui, J.; Niu, Q. J., Asymmetric polyamide nanofilms with highly ordered nanovoids for water purification. *Nat Commun* **2020,** *11*, (1), 6102.
15. Lim, Y. J.; Goh, K.; Lai, G. S.; Zhao, Y.; Torres, J.; Wang, R., Unraveling the role of support membrane chemistry and pore properties on the formation of thin-film composite polyamide membranes. *J. Membr. Sci.* **2021,** *640*, 119805.
16. Zhao, Q.; Zhao, D. L.; Nai, M. H.; Chen, S. B.; Chung, T. S., Nanovoid-Enhanced Thin-Film Composite Reverse Osmosis Membranes Using ZIF-67 Nanoparticles as a Sacrificial Template. *ACS Appl Mater Interfaces* **2021,** *13*, (28), 33024-33033.
17. Kwak, S. Y.; Jung, S. G.; Kim, S. H., Structure-motion-performance relationship of flux-enhanced reverse osmosis (RO) membranes composed of aromatic polyamide thin films. *Environ. Sci. Technol.* **2001,** *35*, (21), 4334-4340.
18. Song, X.; Gan, B.; Qi, S.; Guo, H.; Tang, C. Y.; Zhou, Y.; Gao, C., Intrinsic Nanoscale Structure of Thin Film Composite Polyamide Membranes: Connectivity, Defects, and Structure-Property Correlation. *Environ. Sci. Technol.* **2020,** *54*, (6), 3559-3569.
19. Chai, G.-Y.; Krantz, W. B., Formation and characterization of polyamide membranes

via interfacial polymerization. *J. Membr. Sci.* **1994,** *93*, (2), 175-192.
20. Kim, C. K.; Kim, J. H.; Roh, I. J.; Kim, J. J., The changes of membrane performance with polyamide molecular structure in the reverse osmosis process. *J. Membr. Sci.* **2000,** *165*, (2), 189-199.
21. Liu, M.; Yu, S.; Tao, J.; Gao, C., Preparation, structure characteristics and separation properties of thin-film composite polyamide-urethane seawater reverse osmosis membrane. *J. Membr. Sci.* **2008,** *325*, (2), 947-956.
22. Wei, J.; Liu, X.; Qiu, C.; Wang, R.; Tang, C. Y., Influence of monomer concentrations on the performance of polyamide-based thin film composite forward osmosis membranes. *J. Membr. Sci.* **2011,** *381*, (1-2), 110-117.
23. Xie, W.; Geise, G. M.; Freeman, B. D.; Lee, H.-S.; Byun, G.; McGrath, J. E., Polyamide interfacial composite membranes prepared from m-phenylene diamine, trimesoyl chloride and a new disulfonated diamine. *J. Membr. Sci.* **2012,** *403-404*, 152-161.
24. Karan, S.; Jiang, Z. W.; Livingston, A. G., Sub-10 nm polyamide nanofilms with ultrafast solvent transport for molecular separation. *Science* **2015,** *348*, (6241), 1347-1351.
25. Xu, J.; Yan, H.; Zhang, Y.; Pan, G.; Liu, Y., The morphology of fully-aromatic polyamide separation layer and its relationship with separation performance of TFC membranes. *J. Membr. Sci.* **2017,** *541*, 174-188.
26. Qiu, S.; Wu, L.; Zhang, L.; Chen, H.; Gao, C., Preparation of reverse osmosis composite membrane with high flux by interfacial polymerization of MPD and TMC. *J. Appl. Polym. Sci.* **2009,** *112*, (4), 2066-2072.
27. Choi, W.; Jeon, S.; Kwon, S. J.; Park, H.; Park, Y.-I.; Nam, S.-E.; Lee, P. S.; Lee, J. S.; Choi, J.; Hong, S.; Chan, E. P.; Lee, J.-H., Thin film composite reverse osmosis membranes prepared via layered interfacial polymerization. *J. Membr. Sci.* **2017,** *527*, 121-128.
28. Maruf, S. H.; Greenberg, A. R.; Ding, Y., Influence of substrate processing and interfacial polymerization conditions on the surface topography and permselective properties of surface-patterned thin-film composite membranes. *J. Membr. Sci.* **2016,** *512*, 50-60.
29. Yun, S. H.; Ingole, P. G.; Kim, K. H.; Choi, W. K.; Kim, J. H.; Lee, H. K., Properties and performances of polymer composite membranes correlated with monomer and polydopamine for flue gas dehydration by water vapor permeation. *Chem. Eng. J.* **2014,** *258*, 348-356.
30. Park, S.-J.; Kwon, S. J.; Kwon, H.-E.; Shin, M. G.; Park, S.-H.; Park, H.; Park, Y.-I.; Nam, S.-E.; Lee, J.-H., Aromatic solvent-assisted interfacial polymerization to prepare high performance thin film composite reverse osmosis membranes based on hydrophilic supports. *Polymer* **2018,** *144*, 159-167.
31. Ma, X.-H.; Yao, Z.-K.; Yang, Z.; Guo, H.; Xu, Z.-L.; Tang, C. Y.; Elimelech, M., Nanofoaming of Polyamide Desalination Membranes To Tune Permeability and Selectivity. *Environ. Sci. Technol. Lett.* **2018,** *5*, (2), 123-130.
32. Song, X.; Gan, B.; Yang, Z.; Tang, C. Y.; Gao, C., Confined nanobubbles shape the surface roughness structures of thin film composite polyamide desalination membranes. *J. Membr. Sci.* **2019,** *582*, 342-349.
33. Ma, X.; Yang, Z.; Yao, Z.; Guo, H.; Xu, Z.; Tang, C. Y., Tuning roughness features of thin film composite polyamide membranes for simultaneously enhanced permeability, selectivity and anti-fouling performance. *J. Colloid Interface Sci.* **2019,** *540*, 382-388.
34. Peng, L. E.; Yao, Z.; Liu, X.; Deng, B.; Guo, H.; Tang, C. Y., Tailoring Polyamide Rejection Layer with Aqueous Carbonate Chemistry for Enhanced Membrane Separation: Mechanistic Insights, Chemistry-Structure-Property Relationship, and Environmental Implications. *Environ. Sci. Technol.* **2019,** *53*, (16), 9764-9770.
35. Peng, L. E.; Yao, Z.; Yang, Z.; Guo, H.; Tang, C. Y., Dissecting the Role of Substrate on the Morphology and Separation Properties of Thin Film Composite Polyamide Membranes: Seeing Is Believing. *Environ. Sci. Technol.* **2020,** *54*, (11), 6978-6986.
36. Peng, L. E.; Jiang, Y.; Wen, L.; Guo, H.; Yang, Z.; Tang, C. Y., Does interfacial vaporization of organic solvent affect the structure and separation properties of polyamide RO membranes? *J. Membr. Sci.* **2021,** *625*, 119173.
37. Peng, L. E.; Yang, Z.; Long, L.; Zhou, S.; Guo, H.; Tang, C. Y., A critical review on

porous substrates of TFC polyamide membranes: Mechanisms, membrane performances, and future perspectives. *J. Membr. Sci.* **2022,** *641*, 119871.
38. Grzebyk, K.; Armstrong, M. D.; Coronell, O., Accessing greater thickness and new morphology features in polyamide active layers of thin-film composite membranes by reducing restrictions in amine monomer supply. *J. Membr. Sci.* **2021**, DOI: 10.1016/j.memsci.2021.120112.
39. Khorshidi, B.; Thundat, T.; Fleck, B. A.; Sadrzadeh, M., Thin film composite polyamide membranes: parametric study on the influence of synthesis conditions. *RSC Advances* **2015,** *5*, (68), 54985-54997.
40. Matthews, T. D.; Yan, H.; Cahill, D. G.; Coronell, O.; Mariñas, B. J., Growth dynamics of interfacially polymerized polyamide layers by diffuse reflectance spectroscopy and Rutherford backscattering spectrometry. *J. Membr. Sci.* **2013,** *429*, 71-80.
41. Song, Y.; Sun, P.; Henry, L.; Sun, B., Mechanisms of structure and performance controlled thin film composite membrane formation via interfacial polymerization process. *J. Membr. Sci.* **2005,** *251*, (1-2), 67-79.
42. Mi, B.; Coronell, O.; Marinas, B.; Watanabe, F.; Cahill, D.; Petrov, I., Physico-chemical characterization of NF/RO membrane active layers by Rutherford backscattering spectrometry☆. *J. Membr. Sci.* **2006,** *282*, (1-2), 71-81.
43. Lin, L.; Feng, C.; Lopez, R.; Coronell, O., Identifying facile and accurate methods to measure the thickness of the active layers of thin-film composite membranes – A comparison of seven characterization techniques. *J. Membr. Sci.* **2016,** *498*, 167-179.
44. Freger, V., Nanoscale heterogeneity of polyamide membranes formed by interfacial polymerization. *Langmuir* **2003,** *19*, (11), 4791-4797.
45. Coronell, O.; Marinas, B. J.; Cahill, D. G., Depth heterogeneity of fully aromatic polyamide active layers in reverse osmosis and nanofiltration membranes. *Environ. Sci. Technol.* **2011,** *45*, (10), 4513-20.
46. Nowbahar, A.; Mansard, V.; Mecca, J. M.; Paul, M.; Arrowood, T.; Squires, T. M., Measuring Interfacial Polymerization Kinetics Using Microfluidic Interferometry. *J. Am. Chem. Soc.* **2018,** *140*, (9), 3173-3176.
47. Yang, Z.; Sun, P. F.; Li, X.; Gan, B.; Wang, L.; Song, X.; Park, H. D.; Tang, C. Y., A Critical Review on Thin-Film Nanocomposite Membranes with Interlayered Structure: Mechanisms, Recent Developments, and Environmental Applications. *Environ. Sci. Technol.* **2020,** *54*, (24), 15563-15583.
48. Kattula, M.; Ponnuru, K.; Zhu, L.; Jia, W.; Lin, H.; Furlani, E. P., Designing ultrathin film composite membranes: the impact of a gutter layer. *Sci Rep* **2015,** *5*, 15016.
49. Wijmans, J. G.; Hao, P., Influence of the porous support on diffusion in composite membranes. *J. Membr. Sci.* **2015,** *494*, 78-85.
50. Jiang, Z.; Karan, S.; Livingston, A. G., Water Transport through Ultrathin Polyamide Nanofilms Used for Reverse Osmosis. *Adv. Mater.* **2018,** *30*, (15), 1705973.
51. Park, H. B.; Kamcev, J.; Robeson, L. M.; Elimelech, M.; Freeman, B. D., Maximizing the right stuff: The trade-off between membrane permeability and selectivity. *Science* **2017,** *356*, (6343), eaab0530.
52. Yang, Z.; Guo, H.; Tang, C. Y. Y., The upper bound of thin-film composite (TFC) polyamide membranes for desalination. *J. Membr. Sci.* **2019,** *590*, 117297.
53. Geise, G. M.; Park, H. B.; Sagle, A. C.; Freeman, B. D.; McGrath, J. E., Water permeability and water/salt selectivity tradeoff in polymers for desalination. *J. Membr. Sci.* **2011,** *369*, (1-2), 130-138.
54. Freeman, B. D., Basis of permeability/selectivity tradeoff relations in polymeric gas separation membranes. *Macromolecules* **1999,** *32*, (2), 375-380.
55. Yang, Z.; Long, L.; Wu, C.; Tang, C. Y., High Permeance or High Selectivity? Optimization of System-Scale Nanofiltration Performance Constrained by the Upper Bound. *ACS ES&T Engineering* **2021**, DOI: 10.1021/acsestengg.1c00237.
56. Loo, S. L.; Fane, A. G.; Krantz, W. B.; Lim, T. T., Emergency water supply: a review of potential technologies and selection criteria. *Water Res.* **2012,** *46*, (10), 3125-51.
57. Bernstein, R.; Belfer, S.; Freger, V., Toward Improved Boron Removal in RO by

Membrane Modification: Feasibility and Challenges. *Environ. Sci. Technol.* **2011,** *45*, (8), 3613-3620.
58. Kanel, S. R.; Manning, B.; Charlet, L.; Choi, H., Removal of arsenic(III) from groundwater by nanoscale zero-valent iron. *Environ. Sci. Technol.* **2005,** *39*, (5), 1291-1298.
59. He, Y. R.; Tang, Y. P.; Ma, D. C.; Chung, T. S., UiO-66 incorporated thin-film nanocomposite membranes for efficient selenium and arsenic removal. *J. Membr. Sci.* **2017,** *541*, 262-270.
60. Guo, H.; Peng, L. E.; Yao, Z. K.; Yang, Z.; Ma, X. H.; Tang, C. Y. Y., Non-Polyamide Based Nanofiltration Membranes Using Green Metal-Organic Coordination Complexes: Implications for the Removal of Trace Organic Contaminants. *Environ. Sci. Technol.* **2019,** *53*, (5), 2688-2694.
61. Fujioka, T.; Kodamatani, H.; Nghiem, L. D.; Shintani, T., Transport of N-Nitrosamines through a Reverse Osmosis Membrane: Role of Molecular Size and Nitrogen Atoms. *Environ. Sci. Technol. Lett.* **2019,** *6*, (1), 44-48.